LA-UR- 09-01729

Approved for public release;
distribution is unlimited.

Title:	The Extended Family of Hexagonal Molybdenum Oxide
Author(s):	H.J. Lunk, H. Hartl, T.A. Frisk, I. Shenderovich, D. Mauder, M. Feist, M.F.G. Fait, M.A. Hartl, L.L. Daemen, and R. Eckelt
Intended for:	J-SOL. ST. CHEM

Los Alamos
NATIONAL LABORATORY
EST. 1943

Form 836 (7/06)

The Extended Family of Hexagonal Molybdenum Oxide

H.-J. Lunk*, H. Hartl**, T.A. Frisk*, I. Shenderovich**, D. Mauder**,
M. Feist***, M.F.G. Fait****, M.A. Hartl*****, L.L. Daemen*****, R. Eckelt****

*Global Tungsten and Powders Corp. , Towanda, USA

**Freie Universität Berlin, Germany

***Humboldt-Universität Berlin, Germany

****Berlin Branch of Leibniz Institute for Catalysis, Germany

*****National Laboratory, Los Alamos, USA

Abstract

Over the last 40 years, a large number of isostructural compounds in the system MoO_3-NH_3-H_2O have been published. The reported molecular formulae of "hexagonal molybdenum oxide" (*HEMO*) varied from MoO_3, $MoO_3 \cdot 0.33NH_3$, $MoO_3 \cdot nH_2O$ ($0.09 \leq n \leq 0.69$) to $MoO_3 \cdot mNH_3 \cdot nH_2O$ ($0.09 \leq m \leq 0.20$; $0.18 \leq n \leq 0.60$).

Samples, prepared by the acidification route, were investigated using thermal analysis coupled on-line to a mass spectrometer for evolved gas analysis; X-ray powder diffraction; Fourier Transform Infrared, Raman and Magic-Angle-Spinning ^{1}H-NMR spectroscopy; Incoherent Inelastic Neutron Scattering. The X-ray study of a selected monocrystal confirmed the presence of the well-known framework of edge-sharing MoO_6 octahedra: Space group $P6_3/m$, $a = 10.527(1)$, $c = 3.7245(7)$ Å, $\gamma = 120°$. The structure of the synthesized samples can best be described by the structural formula $(NH_4)[Mo_x\square_{1/2+p/2}(O_{3x+1/2-p/2})(OH)_p] \cdot yH_2O$ ($x = 5.9$-7.1; $p \sim 0.1$; $y = 1.2$-2.6), which is consistent with the existence of one vacancy for 12-15 molybdenum sites.

The "chimie douce" reaction of $MoO_3 \cdot 0.155NH_3 \cdot 0.440H_2O$ with a 1:1 mixture of NO/NO_2 at 100 °C resulted in the synthesis of $MoO_3 \cdot 0.539H_2O$.

Tailored nano-sized molybdenum powders can be produced using *HEMO* as precursor.

Keywords

Hexagonal molybdenum oxide, "chimie douce" reaction, SEM, XRD, TA-MS, FTIR, IINS, MAS-^{1}H-NMR

Introduction

Transition metal oxides such as molybdenum trioxide, MoO_3, and tungsten trioxide, WO_3, have drawn much attention due to their variety of crystalline phases and their inherent chromogenic properties. These oxides are useful in the fabrication and development of electrochromics, electronic information displays, batteries, optical memory devices, and in sensor device technology [e.g. 1,2]. Recently, research efforts have been focused on the synthesis and characterization of two- and one-dimensional structures such as ultra-thin films, nano-rods, nano-belts and nano-fibers [e.g. 3], which exhibit properties quite different from the bulk properties of the materials.

It is well known that the particular phase of nano-structured MoO_3 is highly dependent on the synthetic route. Molybdenum trioxide exhibits five polymorphs. In addtion to the thermodynamically stable orthorhombic α-MoO_3 with a peculiar 2D layered structure [4], four metastable polymorphs have been discovered. The β-MoO_3 and β'-MoO_3 modifications are monoclinically distorted variants of the 3D ReO_3 structure [5]. The high-pressure modification MoO_3-*II* [6] produces a specific layered phase, different from that of α-MoO_3. The hexagonal phase *h*-MoO_3 ($P6_3/m$ or $P6_3$) allows a versatile intercalation chemistry with interesting chemical, electrochemical, electronic and catalytic properties [e.g. 8]. Nano-sized molybdenum powders can be produced by using this phase as precursor [9,10].

The long and puzzling history of *"hexagonal* MoO_3*"* started in 1906, when Rosenheim described the preparation of a *"molybdic acid hydrate"* [11]. The substance was precipitated by acidification of an aqueous solution of ammonium paramolybdate (APM), $(NH_4)_6[Mo_7O_{24}]\cdot 4H_2O$, with nitric acid. In 1969, Peters et al. utilized Rosenheim's procedure and analyzed the isolated precipitates by chemical and thermal analyses and also by XRD [12]. Depending on the concentration of the starting chemicals APM and HNO_3, the composition of their *"ammonium-C-phase"* $MoO_3\cdot mNH_3\cdot nH_2O$ varied from m = 0.15 to 0.17 and from n = 0.405 to 505; the X-ray diffractograms were identical. The authors indexed all measured reflections and determined the crystal lattice as cubic body-centered (a = 12.98 ± 0.02 Å).

Since 1969, a large number of papers have been published about *"hexagonal* MoO_3*'*. However, several authors overlooked the existing literature and claimed the synthesis of a new phase. The reported overall composition of *"hexagonal molybdenum oxide"* (*HEMO*) varied from MoO_3, $MoO_3\cdot 0.33NH_3$, $MoO_3\cdot nH_2O$ ($0.09 \le n \le 0.69$) to $MoO_3\cdot mNH_3\cdot nH_2O$ ($0.09 \le m \le 0.20$; $0.18 \le n \le 0.60$). These phases, characterized by virtually identical XRD's, can be obtained by thermal decomposition of APM [13,14], by acidification of aqueous solutions of APM or ammonium dimolybdate (ADM), $(NH_4)_2[Mo_2O_7]$ [e.g. 15], by reaction in a sealed tube between MoO_3, NH_3 and H_2O [16] and also from MoO_3 and a mixture of ammonium carbamate and ammonium bicarbonate [17]. Kiss et al. [13] first correctly identified the *HEMO* phase as hexagonal.

Recently, by using the acidification route, even the synthesis of a new cubic heteropolymolybdate with a Keggin-type structure $(NH_4)_2[MoO_4Mo_{12}O_{36}]\cdot 6H_2O$ was claimed, wherein molybdenum allegedly resides in both the tetrahedral hetero as well as the octahedral peripheral atomic positions [9,10]. The published X-ray pattern of the rod-shaped crystals is identical with that of *HEMO*; its overall composition $MoO_3\cdot 0.154NH_3\cdot 0.538H_2O$ lies within the known range of compositions for $MoO_3\cdot mNH_3\cdot nH_2O$.
The publication [18] is an other example of an incomplete literature search and does not characterize the overall composition of the synthesized phase using chemical analysis. In 2009, these authors mistakenly *"report, for the first time, the crystal structure, morphology of hexagonal phase* MoO_3 *nanorods prepared by a simple chemical precipitation route using ammonium paramolybdate"*, though this information has been known for many years.

The hexagonal phase has been verified also for *HEMO* compositions, containing Na, K, Rb, Cs or Ag cations instead of $[NH_4]^+$ [e.g. 19] and also for compounds like $H_{0.13}V_{0.13}MoO_{0.87}O_3 \cdot 3H_2O$ [20], where part of molybdenum is occupied by vanadium.

All the molybdenum atoms in the structure of *HEMO*, discussed above, are in the +6 oxidation state. By using hydroxylamine hydrochloride as a reducing agent, the hexagonal ammonium molybdenum *bronze* $NH_4Mo_6O_{18}$ [= $(NH_4)_{0.17}MoO_3$] was synthesized, producing molybdenum atoms with an average oxidation state of +5.83 [21].

The objective of this work is to dispel the confusion which has arisen in the literature concerning the identity of *HEMO* phases variously described. A comprehensive characterization of theses materials will lead to a better understanding of the structure of $MoO_3 \cdot mNH_3 \cdot nH_2O$, whose composition can vary over a relatively wide range. The tailored synthesis of this phase has the potential for being utilized as material for intercalation chemistry and different catalytic applications. Its reduced form can be used as a starting material for making nano-sized molybdenum metal powder and molybdenum carbide powders [9,10].

Experimental

A. Preparation

The preparation followed the route, taken by the authors of [10]. The starting chemical, ADM, was manufactured at GTP in Towanda, PA. Its trace element concentrations in ppm were as follows: Ca, Mg <1; Mn, Ni <2; Al, Cr, Cu, Fe <4; Na <5; Pb <6; As, Si, Sn, P <8; W 65; K 95. The Apparent Scott Density amounted to 1.34 g/cm^3. An amount of 38 g ADM was dissolved in 400 mL deionized water and heated to about 70ºC. While agitating the solution with a magnetic stirrer, 150 mL aqua regia (3 parts 12N HCl, 1 part 14N HNO_3, by volume) were added. Then 100 mL of a diluted aqueous ammonia solution (1 part 14N NH_3 to 1 part water) was added, while continuously stirring. The clear solution had a light yellow color and the desired phase was precipitated by adding 40 mL 14 N HNO_3, while continuously stirring. The solution was heated at 70ºC for another 5 to 10 minutes and then left to crystallize. After about 15 minutes, a colorless precipitate formed. The precipitate was left in the mother liquor over night and then isolated by filtration. The precipitate was washed once with 200 mL of 0.1N HNO_3 and three times with deionized water and then dried at 110ºC. Alternatively, the precipitate was fabricated using only 3.3N HCl, instead of aqua regia.

B. Instrumentation

The dried precipitates were characterized by chemical analysis, scanning electron microscopy (SEM), X-ray diffraction (XRD), Thermal analysis coupled on-line by a *Skimmer®* system to a quadrupole mass spectrometer for evolved gas analysis (TA-MS), Fourier-Transform Infrared (FTIR), Raman and Magic-Angle-Spinning (MAS) ^{1}H-NMR spectroscopy and also by Incoherent Inelastic Neutron Scattering (IINS).

For determining the molar composition $MoO_3 \cdot mNH_3 \cdot nH_2O$ of the precipitated samples, two independent <u>analytical measurements</u> were needed. The content of NH_3 was determined by the classical Kjeldahl method [22]. The samples were distilled using a KJELTEC System 1026 Distilling Unit, whereby 0.1 g to 0.5 g of the sample were placed into a 100 mL distilling flask to which 10mL of water and 20mL of 10N NaOH was added. The sample was then distilled through steam generation for 3.7 minutes. The ammonia distillate was collected in a 20 mL solution of saturated boric acid. The collected solution was

then titrated on a Mettler DL-67 auto-titrator using 0.4N HCl. By using a Mettler small furnace (SF1100) TGA/SDTA 851e instrument, the mass loss of ~10 g sample sizes heated in air up to 550°C provides the sum of H_2O and NH_3. The content of H_2O was calculated as difference of the overall mass loss less the content of NH_3.

The Hitachi S-3000N *scanning electron microscope (SEM)* was used to acquire images of the powders at an accelerating voltage of 3kV and a magnification of 5000x.

For the *X-ray powder diffraction* measurements a Rigaku D/Max Vertical Goniometer diffractometer was employed. The experimental conditions were as follows: scan range 6 to 70 degrees 2-theta; step size 0.02 degrees 2-theta; dwell time 1 second.

The *X-ray single crystal structure determination* and the diffracted intensities were measured on a Bruker XPS diffractometer: CCD area detector; MoK_α radiation ($\lambda = 0.71073$ Å; graphite monochromator); T = 173 K; structure solution: Empirical absorption correction (SADABS). The structure was solved by direct methods and refined based on F^2 data with a least-squares procedure using the WinGX program system [23]. Anisotropic displacement parameters were assigned to all non-hydrogen atoms; hydrogen atoms could not be located.

The TA-MS analysis was performed using a thermal analyzer STA 409C (Netzsch Gerätebau GmbH, Selb/Germany), which was coupled to a quadrupole mass spectrometer (QMG 422, Balzers). The conditions were: 70 mL·min^{-1} air flow; 5 K·min^{-1} heating rate; about 50 mg sample mass; corundum crucibles. The overlapping individual steps have been distinguished by their minima in the DTG curve. The ion current (IC) curves for the selected ions with m/z = 15 (NH^+), 17 (OH^+; NH_3^+), and 18 (H_2O^+) were recorded in the multiple ion detection (MID) mode.

The "chimie douce" reaction of *HEMO* with NO/NO_2 was performed in an integral fixed bed reactor made from fused silica (i.d. 10 mm; isothermal heating zone 50 mm; PID controller) at 100 °C; sample mass 1.00 g. The educt feed was a 1:1 mixture of NO and NO_2 (diluted in He, each: 0.5%, 20 mL·min^{-1}) in He (30 mL·min^{-1}). Before feeding the reactor with the reaction gas mixture, the sample was treated in He at 100 °C for 2-3 hours to equilibrate the educt flow and to stabilize the multi gas sensor. After the desired reaction time the educt mixture was replaced by helium. The composition of the educt and product stream was analyzed by an on-line multi gas sensor for the simultaneous analysis of NO and NO_2.

The FTIR spectra were acquired on a Nicolet Magna 760 spectrometer. The samples were diluted in KBr at a mass ratio of 1:15 using a KBr beamsplitter and a DTGS detector. They were analyzed using the Diffuse Reflectance Infrared Fourier-Transform (DRIFT) component. Each FTIR spectrum is a composite of 512 scans at a resolution of 4 cm^{-1}.

The Raman spectra were acquired using a Nicolet 590 Raman module. The samples were analyzed neat in NMR tubes using a CaF_2 beamsplitter and an InGaAs detector. The spectra were acquired using a laser beam of 1.16 W and a resolution of 4 cm^{-1}. Each spectrum was composed of 128 scans.

Incoherent Inelastic Neutron Scattering (IINS) data were collected at a temperature of 10 K on the Filter Difference Spectrometer (FDS) at the LANSCE facility at Los Alamos National Laboratory. This instrument is used for vibrational spectroscopy through incoherent inelastic neutron scattering. The instrument is designed for high count rates using a large solid-angle (3 steradians) detector. The samples were loaded in cylindrical aluminum cans (20 mm outer diameter, 2 mm wall thickness, 100 mm height) in a helium atmosphere to ensure good thermal contact with the closed-cycle refrigerator. After a short temperature equilibration time, a vibrational spectrum was collected over a period of 12 hours.

Solid-state high-resolution ^{1}H-NMR spectroscopy: Single-pulse experiments with high-speed Magic-Angle-Spinning (MAS). The NMR spectra were measured at room temperature.

Varian spectrometer: 600 MHz (14.1 T), equipped with Varian 3.2 mm probe; MAS rotational frequency: 20 kHz; 90 ° pulse length: 1.3 µs; pulse delay: 4 s; number of scans: 256; external reference: adamantane (1.74 ppm from TMS).

Results and Discussion

The preparation of *HEMO* was carried out by using ADM as starting material and alternatively aqua regia and HCl alone. The data from the chemical analysis and X-ray charactyerization are compiled in Table I.

Table I: Overall composition and X-ray characterization of *h-MoO_3* samples

Sample	Preparation	NH_3 (%)	$MoO_3 \cdot mNH_3 \cdot nH_2O$			*a* (Å)	*c* (Å)	I_{100} (Å) $I_{80\text{-}40}$ (Å)
			m	n	m + n			
h-MoO_3-1	ADM + aqua regia	1.58	0.143	0.440	0.583	10.58	3.73	3.44 100 9.04 50
h-MoO_3-1-300	h-MoO_3-1 heated at 300ºC	1.59	0.141	0.253	0.394	10.58	3.72	3.45 100 9.15 60
h-MoO_3-1-320	h-MoO_3-1 heated at 320ºC	1.32	0.116	0.211	0.327	10.59	3.73	3.45 100 9.07 60
h-MoO_3-1-P	h-MoO_3-1 kept over P_4O_{10}	1.70	0.153	0.372	0.525	10.58	3.73	3.44 100 8.98 40
h-MoO_3-1-NH_3	Ammoniated h-MoO_3-1-P	3.57	0.326	0.343	0.669	10.54	3.73	3.43 100 8.93 50
h-MoO_3-2	ADM + aqua regia	1.71	0.155	0.440	0.595	10.56	3.73	3.44 100 9.06 40
h-MoO_3-2-NOX	h-MoO_3-2 + NO/NO_2	<0.2	0.000	0.539	0.539	10.59	3.72	3.44 100 9.06 40
h-MoO_3-3	ADM + HCl	1.85	0.169	0.479	0.648	10.57	3.73	3.45 100 9.09 40
h-MoO_3-4		1.82	0.161	0.243	0.404	10.59	3.72	3.46 100 9.04 30
h-MoO_3-5	Commercial product	1.88	0.168	0.295	0.463	10.57	3.73	3.45 100 9.12 80

The scanning electron microscopy (SEM) data of sample *h-MoO_3-1* is shown in Figure 1. The crystals have the shape of straight hexagonal rods.

The X-ray diffractogram of sample *h-MoO_3-1* is shown in Figure 2. It is evident that the material is well-crystallized and single-phased. All the observed reflections can be indexed in hexagonal symmetry, with interplanar spacings reported for *h-MoO_3* [8]. All samples presented in Table I are characterized by an X-ray diffractogram virtually identical with that presented in Figure 2. The structure remained unchanged, even after heating the sample *h-MoO_3-1* up to 320ºC and loading it with gaseous ammonia. The cell parameter *a*, determined from the powder XRD's, varies from 10.54 to 10.59 Å; parameter *c* amounted to 3.72-3.73 Å.

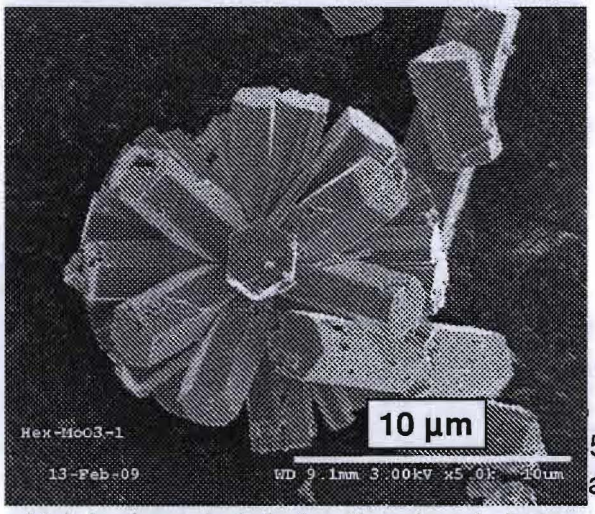

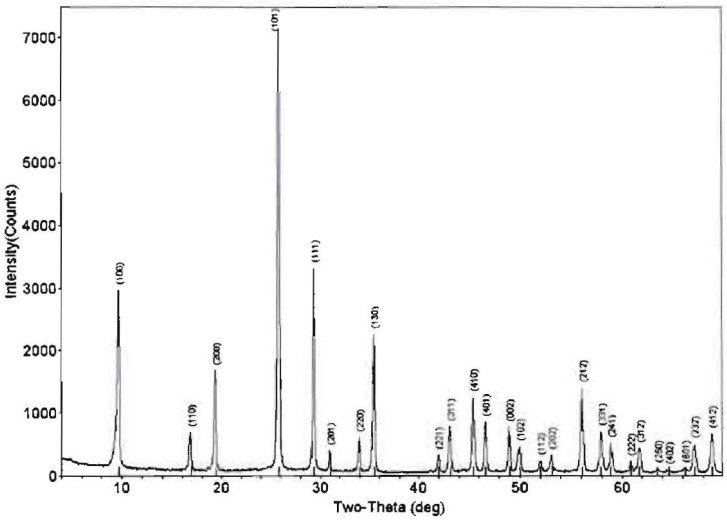

Fig. 2: XRD of h-MoO_3-1

h-MoO_3-1 confirmed the presence of the well-known first determined for hexagonal *$KMo_5O_{15}OH{\cdot}2H_2O$* [24]: 5(7) Å, $\gamma = 120°$ (Figure 3). The tunnels that are formed by ameter of 5-6 Å (Figure 4) and show an electron density, which is characteristic for disordered nitrogen or oxygen atoms in the tunnels. The shortest O....O distance between diagonally located O-atoms is 5.96 Å. An inserted cylinder would have a diameter of 5.65 Å. After subtracting the twofold van-der-Waals radius of O or O^{2-}, the diameter of the inserted cylinder would shrink to 2.5-3.0 Å. The mean N....O or O....O distance of 2.98 Å corresponds with the length of the hydrogen bonds N–H....O and O–H....O.

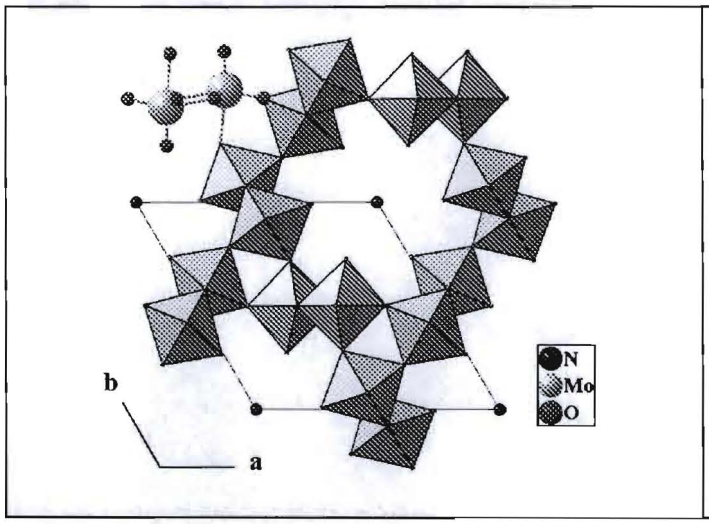

Fig. 3: Polyhedral representation of the *h-MoO_3* framework with nitrogen at the unit cell vertices

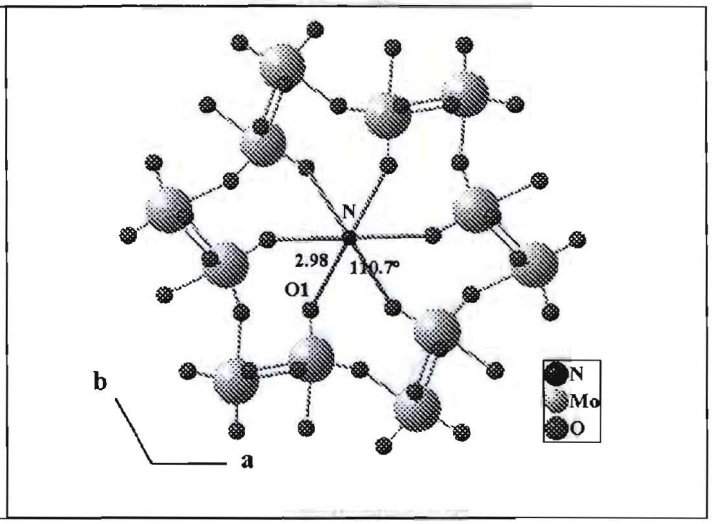

Fig. 4: Ball and stick representation of the *h-MoO_3* framework viewed from the 001 direction

The thermal behavior of *h-MoO_3-1* in air is characterized by a sequence of three, possibly four (cf. the two sub-maxima in the first broad peak, Figure 5) consecutive steps that more or less strongly overlap. All steps are caused by the release of water, while the latter two also show an ammonia liberation with maxima around 340 and 410 °C. Due to the low amount of ammonia that is released above 280ºC, the intensity ratio, m17 : m18, cannot be used to precisely determine the amount of liberated ammonia. However, the m15 trace unambiguously demonstrates the release of ammonia above 280ºC.

The thermal characteristics confirmed that the rate of decomposing and removing $[NH_4]^+$ ions is less than that of neutral water molecules at relatively low temperatures. The dehydration of *h-MoO3-1* at 300ºC or over P_4O_{10} confirmed this finding; the dehydration at 320ºC caused a 18% loss of ammonium (cf. Table I). The general character of the first three mass loss steps is endothermic as expected (more clearly observed in argon, but not discussed in this presentation), even if the peaks are weak and poorly expressed. This is obviously due to the usage of corundum crucibles which are preferred when measuring in air (cf. [25] where the exothermicity of DTA traces had been attributed to the catalytic burning of ammonia in the presence of platinum as crucible material). The third mass loss with the sharp DTG peak at 425 °C is strongly exothermic, which is attributed to the recrystallization of the decomposed parent phase to *α-MoO3*. The light gray residue was identified by XRD as orthorhombic *α-MoO3*. Regarding the general curve shape of the TG and DTG traces, the behavior in argon is quite similar except a somewhat greater mass loss for the temperatures above 250 °C (4.04 vs. 2.68 %). In argon, the liberated ammonia acts as an reducing agent. The blue-colored residue contains also the molybdenum suboxide Mo_4O_{11}, in addition to the main component *α-MoO3*.

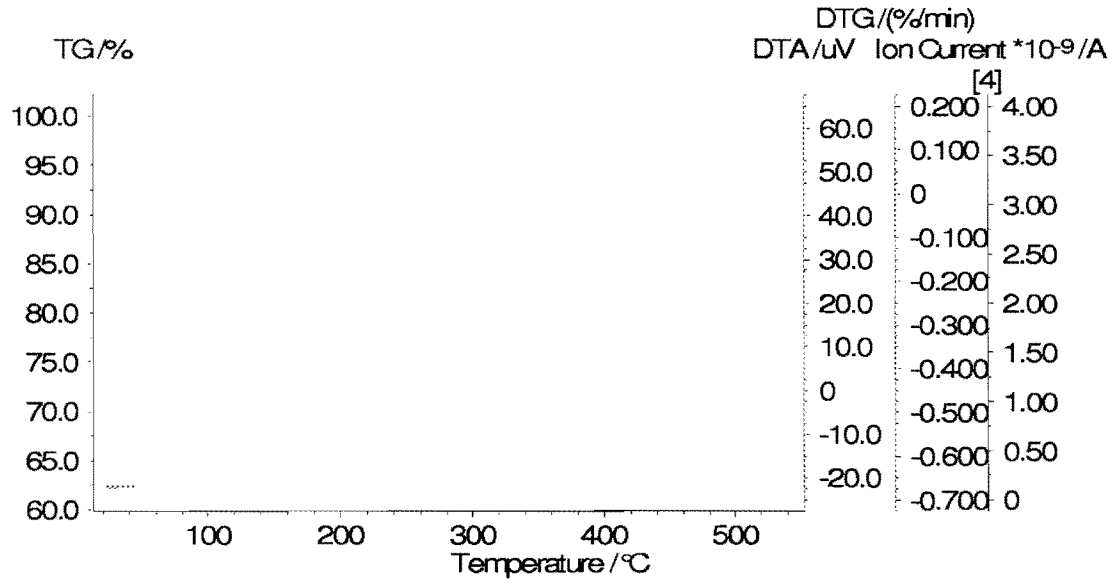

Fig. 5: TA-MS curves of h-MoO_3-1 in air with the ion current (IC) curves for the mass numbers m/z=15 ($^{15}N^+$), 17 ($^{14}NH_3^+$, OH^+) and 18 (H_2O^+)

The "chimie douce" reaction of *h-MoO3-2* with a 1:1 mixture of NO and NO_2 at 100 °C (cf. Section *Instrumentation* for experimental details) led to the $[NH_4]^+$-free sample *h-MoO3-2-NOX* (see Table I). Figure 6 reveals that both gases react simultaneously with the starting material. The equimolar mixture of the oxidizing agents NO (oxidation state of N +2) and NO_2 (oxidation state of N +4) is the ideal oxidant for the oxidation of $[NH_4]^+$ (oxidation state of N -3) to N_2 with and oxidation state of ±0. The resultant compound is characterized by an X-ray pattern, virtually identical to that of the starting material. The characterization of *h-MoO3-2-NOX* by FTIR / Raman spectroscopies, and IINS is presented below. From a mechanistic standpoint, the applied "chimie douce" route at 100 °C with an equimolar mixture of NO and NO_2 represents a less complex gas-solid reaction than the use of NO_2 alone at 250 °C [26]. The transformation of *h-MoO3-2* into *h-MoO3-2-NOX* requires certain structural rearrangements to eliminate the Mo vacancies in the parent material.

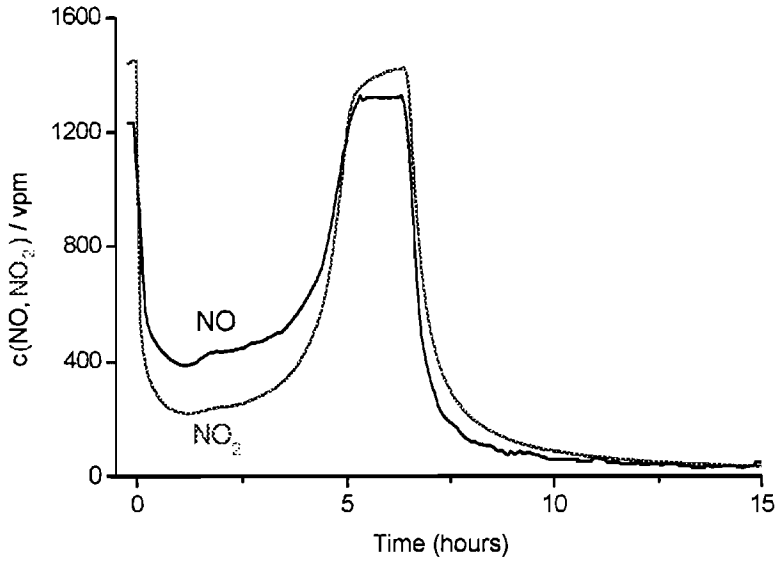

Fig. 6: "Chimie douce" reaction of h-MoO_3-2 with a 1:1 mixture of NO/NO_2 at 100 °C

The FTIR spectrum of h-MoO_3-2 is shown in Figure 7; its *Raman spectrum* is in Figure 8. The bands at 3527 and 1607 cm^{-1} can be attributed to the OH stretching and deformation vibrations of hydrated water, respectively. The bands at 3228 and 1435 cm^{-1} agree with the frequencies of the stretching and deformation vibrations of $[NH_4]^+$ ions [27]. In the range below 1000 cm^{-1}, the spectrum shows relatively sharp bands at 971 cm^{-1} and 914 $cm^{-1}$and a broad absorption from 700 to 500 cm^{-1}, which can be assigned to Mo-O bond stretching and bending vibrations and to the vibrational motion of H_2O. The Raman spectrum also shows the sharp band at 973 cm^{-1} and the broad band at 900 cm^{-1}. Additional bands are observed in the range from 700 to 100 cm^{-1}.

The FTIR spectrum of h-MoO_3-2-NOX clearly indicates that ammonium ions are not present in that sample. The characteristic bands at 3228 and 1435 cm^{-1} are absent. These findings agree with the results of chemical analysis (cf. Table I). Compared to the parent material, the *Raman spectrum* of the $[NH_4]^+$-free sample shows a bathochromic shift of the band at 973 cm^{-1} to 981 cm^{-1}.

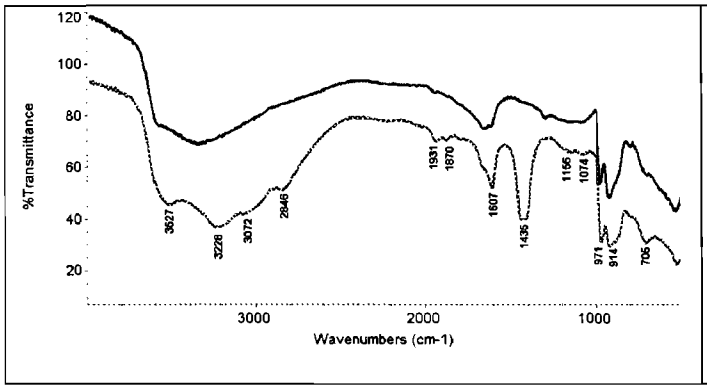

Fig. 7: FTIR spectra of h-MoO_3-2 (red) and h-MoO_3-2-NOX (blue)

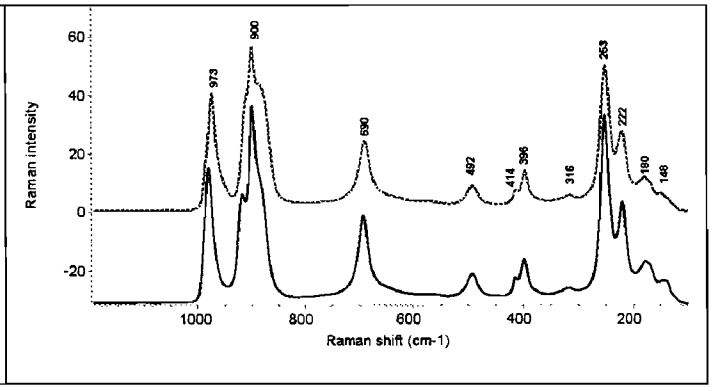

Fig. 8: Raman spectra of h-MoO_3-2 and h-MoO_3-2-NOX (blue)

The IINS spectra were background subtracted using vanadium and deconvoluted. The comparison of the hexagonal phases *h-MoO_3-1*, *h-MoO_3-320*, and *h-MoO_3-1-NH_3* (cf. Table I) to *α-MoO_3* is shown in Figures 9 to 11 at low, medium and high wavenumbers, respectively. A detailed view of two of the most

interesting areas is given in Figure 12. The bands that appear in all four samples are due to Mo-O vibrations of the molybdates. The extra bands in the three hexagonal samples are due to vibrations connected with hydrogen.

The assignment of bands to water and ammonium at low wavenumbers was done by comparing the relative intensity of bands for the three hexagonal samples (see Figure 9). Since these samples vary in the amount of ammonia and water they contain, a partial assignment could be done. Librational modes of $[NH_4]^+$ (torsions of the cation on its site) give raise to bands at 320 and 359 cm^{-1} comparable to those found in e.g. ammonium bromide, $[NH_4]Br$ [28]. ~~These modes are also visible in our spectra (marked with MB), but their intensity is comparably small.~~

Figure 10 shows the spectra in the medium wavenumber region. The librational bands for "free" water, i.e. water that is neither complexed nor bound or adsorbed, are usually visible between 450 and 1000 cm^{-1} [29] (black box in Figure 10). To clarify the graph, a straight line is drawn underneath each spectrum as background in the respective color. Only in the sample with most water (*h-MoO3-1*), a large area corresponding to free water is clearly visible (arrow). After drying the sample over P_4O_{10} and loading it with dry gaseous ammonia, the free water seems to have been removed. The remaining water is either strongly adsorbed on the tunnel surface or has reacted with the surface to form an aquo- or hydroxo-metal complex.

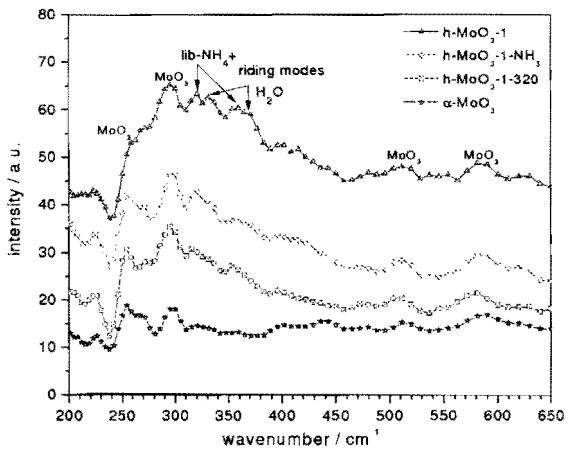

Fig. 9: IINS spectra of hexagonal and orthorhombic MoO_3 (low wavenumber region)

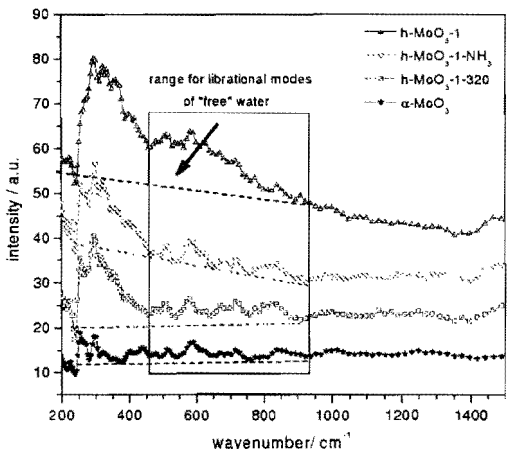

Fig. 10: IINS spectra of hexagonal and orthorhombic MoO_3 (medium wavenumber region)

Figure 11 gives an overview of the high wavenumber region. There is intensity visible in the expected areas for $[NH_4]^+$ ions: N-H deformations (1380-1550 cm^{-1}: scissor at 1680 cm^{-1}, umbrella mode at 1400 cm^{-1}) and N-H stretch (3050-3350 cm^{-1}). For "free" ammonia NH_3, the N-H stretch and N-H scissor modes would be shifted to higher wave numbers (3223-3378 cm^{-1} and 1646 cm^{-1}, respectively). The umbrella mode, a very intense mode, should appear at 1060 cm^{-1}. We do see intensity at this region for *h-MoO3-1-NH3* at 1080 cm^{-1}. Furthermore, a band at 800 cm^{-1} occurs as a shoulder in the same spectrum. This band could correspond to the rocking mode for NH_3, which occurs in the region 590-950 cm^{-1}. These observations agree with what we expected from the preparation route of this "ammoniated" sample.

Figure 12 is an enlarged section of the range 2800 to 3800 cm^{-1} where the N-H and O-H stretch frequencies appear. The data of the *HEMO* were treated slightly differently than before. The background that was subtracted from the sample spectra was the orthorhombic *α-MoO3* spectrum

instead of the standard background vanadium. This can be done since at high wavenumbers there are no phonon or lattice vibrations that differ in hexagonal and orthorhombic molybdate phases. By subtracting *α-MoO3*, all Mo-O vibrational bands are eliminated leaving the Mo-O-H and Mo-N-H vibrations more visible. The data points were connected using a cubic spline function to make the bands more distinguishable. The sample with the highest level of water, *h-MoO3-1*, shows a large broad band from 3400 to 3800 cm^{-1}. This is common for lattice water (3200-3600 cm^{-1}: H-O-H stretch). The samples *h-MoO3-1-NH3* and *h-MoC3-1-320* show a prominent band at 3480 cm^{-1} that indicates water strongly coordinated on a metal. The metal ion's charge and mass shifts the frequencies to lower wavenumbers. There are vibrational bands for N-H stretch in the region for $[NH_4]^+$ (3050-3350 cm^{-1}). The two N-H stretch vibrations of $[NH_4]^+$ shift to lower wave numbers from *h-MoO3-1-NH3* (3220 and 3097 cm^{-1}), *h-MoO3-1* (3170 and 3033 cm^{-1}) to *h-MoO3-1-320* (3101 and 2982 cm^{-1}).

The partially dehydrated samples *h-MoO3-1-320* and *h-MoO3-1-NH3* are characterized by the near absence of clear librational bands for (nearly free) hydrogen-bonded water. On the other hand, the free water is only visible in *h-MoO3-1* (cf. Figure 10). Water in the other two hexagonal samples seems to have reacted and formed hydroxyl groups or was adsorbed onto the walls of the tunnels. When looking carefully, there is a sharp peak around 3500 cm^{-1} for *h-MoO3-1-NH3* and *h-MoO3-1-320* (see Figure 12). The band around 3500 cm^{-1} is most likely the O-H stretch in Mo-OH or M-(OH_2) that is shifted to lower wavenumbers due to the heavy metal Mo.

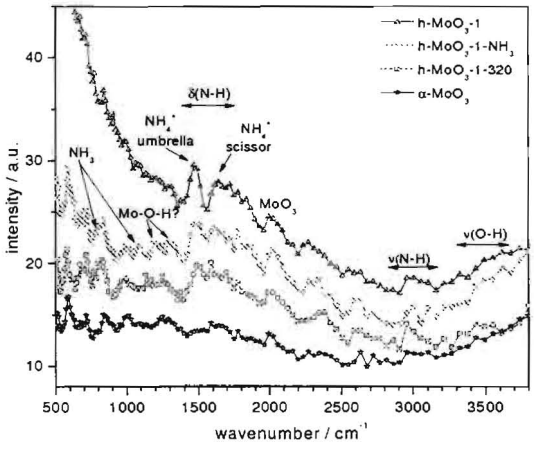

Fig. 11: IINS spectra of hexagonal and orthorhombic MoO_3 (high wavenumber region)

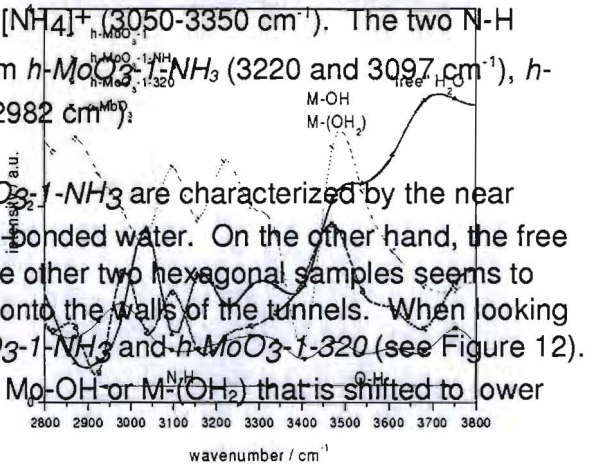

Fig. 12: IINS spectra of hexagonal and orthorhombic MoO_3 (enlarged section of the range 2800 to 3800 cm^{-1})

Due to the position and intensity of the bands, we conclude that there is ammonium $[NH_4]^+$ present. In addition to that, there are weak signals for ammonia in one of the three hexagonal samples, namely *h-MoO3-1-NH3*. The band with the high intensity at 1478 cm^{-1} is the umbrella mode of $[NH_4]^+$. It may be slightly shifted due to recoil. It is too high in frequency to be the umbrella mode of ammonia, NH_3. There is intensity in the spectrum where the $[NH_4]^+$ scissors would be at 1642 cm^{-1}. This band has less intensity than the umbrella mode. The N-H stretch region again shows typical bands for the N-H stretch of ammonium ions, but we also observe N-H stretching bands for ammonia in sample *MoO3-1*-NH_3. A shift of N-H stretch frequencies for ammonium in the three samples was observed. It seems that the $[NH_4]^+$ cations float more or less freely in *h-MoO3-1*, but are more restricted in *h-MoO3-1-NH3*, which is filled with "free" NH_3 (shift of N-H stretch to higher frequency).

The situation in the *HEMO* seems similar to that of a zeolite. The $[NH_4]^+$ cations seem to float freely in the tunnels when the tunnels' surface is hydroxylated or hydrated. The proton of $[NH_4]^+$ hops now and then on Mo-OH, taking advantage of the electron density on the oxygen lone electron pair. If there were significant intermolecular interactions, the librational frequencies would be shifted downward appreciably.

The ^{1}H-NMR spectrum of *h-MoO_3-2* is shown in Figure 13. Line-shape deconvolution (Figure 14) indicates that there are two clearly identified proton-containing environments in the original material. Proton exchange between these two environments is slow, relative to the NMR time scale of milliseconds. One environment is characterized by a relatively narrow peak at 5.8 ppm, another by a broader peak at 6.6 ppm. An extremely weak peak at 1 ppm must be assigned to a third species. Only the peaks at 6.6 ppm and 1 ppm remain in the $[NH_4]^+$-free sample *h-MoO_3-2-NOX* (Figures 15,16). Thus, we conclude that the parent material contains H_2O (resonates at 6.6 ppm), $[NH_4]^+$ (resonates at 5.8 ppm), and OH (resonates at 1 ppm). It is not surprising that the proton exchange between water and $[NH_4]^+$ is slow. The position of the peak we attribute to water (6.6 ppm) is not affected by the presence of the chemical environment we attribute to $[NH_4]^+$. Thus, we assert that all three species are not in contact with each other. Protons of an isolated water molecule resonate around 1 ppm. Hydrogen bonding results in a low field shift, e.g. bulk water resonates at 4.8 ppm at room temperature. Obviously, the present geometry results in a structuring of water molecules and a strengthening of intermolecular hydrogen bonds. The latter effect can be responsible for the observed low field shift compared to bulk water.

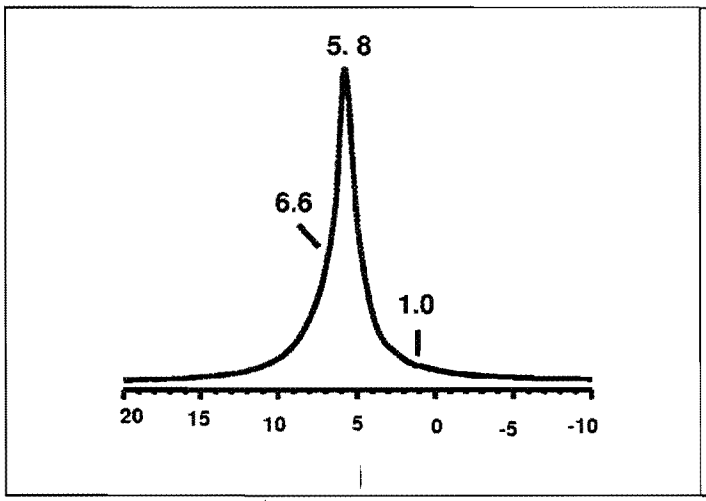

Fig. 13: MAS-^{1}H-NMR spectrum of *h-MoO_3-2*

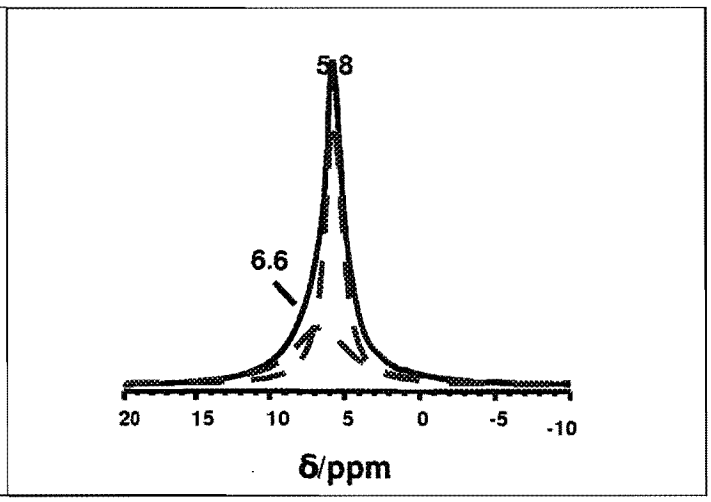

Fig. 14: MAS-^{1}H-NMR spectrum of *h-MoO_3-2* (deconvolution)

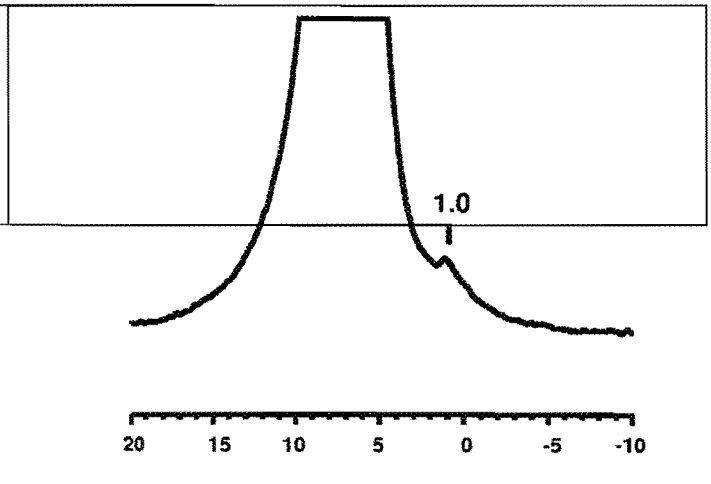

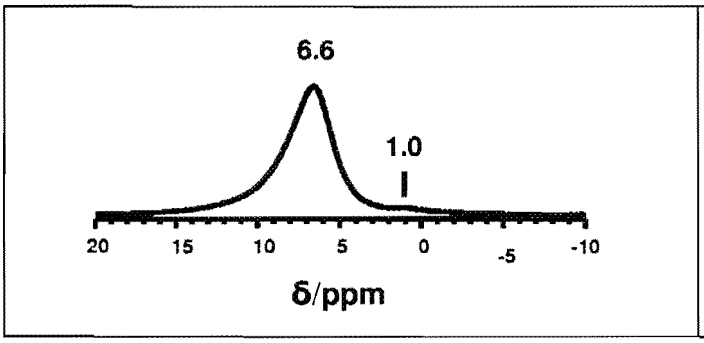

Fig. 15: MAS-^{1}H-NMR spectrum of *h-MoO_3-2-NOX*

Fig. 16: MAS-^{1}H-NMR spectrum of *h-MoO_3-2-NOX* (4x magnification of Fig. 15)

Conclusions

Considering all of the experimental data, the structure of the prepared "hexagonal molybdenum oxide" samples can best be described by the structural formula $(NH_4)[Mo_x\square_{1/2+p/2}(O_{3x+1/2-p/2})(OH)_p] \cdot yH_2O$ ($x = 5.9\text{-}7.1$; $p \sim 0.1$; $y = 1.2\text{-}2.6$), which is consistent with the existence of one vacancy for 12-15 molybdenum sites. The hexagonal *MoO_6* framework accommodate $[NH_4]^+$ cations, which float relatively freely in the tunnels. In the neigborhood of a vacant Mo site the oxygen atoms are partially replaced by coordinated H_2O molecules, isolated H_2O molecules (crystal water) and also OH groups. The new "chimie douce" reaction with NO/NO_2 is able to remove topotactically $[NH_4]^+$ ions at 100ºC from the parent structure. This result demonstrates that the *in situ* oxidation of $[NH_4]^+$ is an elegant route for preparing metastable oxides with tunnels for various applications in the field of batteries and catalysis.

References

1. C.N.R. Rao, and B. Raveau, *Transition Metal Oxides: Structure, Properties, and Synthesis of Ceramic Oxides*, 2nd ed., Wiley-Interscience, 2004

2. K. Hosono, I. Matsubara, N. Murayama, S. Woosuck, and N. Izu, *Chem.Mater.*, **17**, 349-354 (2005)

3. G. Fu, X. Xu, X. Lu, and H. Wan, *J.Am.Chem.Soc.*, **127**, 3989-3996 (2005)

4. L. Kihlborg, *Arkiv Kemi*, **21**, 357-364 (1963)

5. E.M. McCarron III, *J.Chem.Soc.Chem.Commun.*, **1986**, 336-338 (1991)

6. J.B. Parise, E.M. McCarron III, and A.W. Sleight, *Mater.Res.Bull.*, **22**, 803-811 (1987)

7. J. Guo, P. Zavalij, and M.S. Whittingham, *Eur.J.Solid State Inorg.Chem.*, **31**, 833-842 (1994)

8. E.M. McCarron III, and J.C. Calabrese, *J.Solid State Chem.*, **91**, 121-125 (1991)

9. R.P. Singh, T.A. Wolfe, and D.L. Houck, U.S. Patent 6,793,907 (2004), B1

10. R.P. Singh Gaur, and T.A. Wolfe, *Proceedings 2006 Int. Conf. Tungsten, Refract. & Hardmetals VI*, Orlando, FL, pp. 122-131

11. A. Rosenheim, *Z.Anorg.Chem.*, **50**, 320 (1906)

12. H. Peters, L. Till, and K.H. Radeke, *Z.Anorg.Allg.Chem.*, **365**, 14-21 (1969)

13. A.B. Kiss, P. Gadó, I. Asztalos, and A.J. Hegedüs, *Acta Chem.Acad.Scient.Hung.*, **66** [3], 235-249 (1970)

14. J. Weinhold, R.D. Jentoft, and T. Ressler, *Eur.J.Inorg.Chem.*, **2003**, 1058-1071

15. N. Sotani, *Bulletin Chem.Soc. Japan*, **48** [6], 1820-1825 (1975)

16. J.L. Garin, and J.M. Blanc, *J.Solid State Chem.*, **58**, 98-102 (1991)

17. R. Benchrifa, *Ann.Chim.Sci.Mat.*, **32** [3], 277-282 (2007)

18. C.V. Ramana, V.V. Atuchin, I.B. Troitskaia, S.A. Gromilov, V.G. Kostrovsky, and G.B. Saupe, *Solid State Commun.*, **149**, 6-9 (2009)

19. J. Guo, P. Zavalij, and M.S. Whittingham, *J.Solid State Chem.*, **117**, 323-332 (1995)

20. L. Dupont, D. Larcher, F. Portemer, and M. Figlarz, *J.Solid State Chem.*, **121**, 339-349 (1996)

21. C.-C. Jiang, G. Liu, Y.-G. Wei, W. Wang, and S.-W. Zhang, *Inorg.Chem.Commun.*, **2**, 258-260 (1999)

22. G. Jander, and K.F. Jahr, *Massanalyse, Theorie und Praxis der Klassischen und der Elektrochemischen Titrierverfahren*, p. 158, Walter DE Gruyter & Co., Berlin (1959)

23. L.J. Farrugia, *J.Appl.Cryst.*, **32**, 837-838 (1999)

24. B. Krebs, and I. Paulat-Böschen, *Acta Cryst.*, **B32**, 1697-1704 (1976)

25. M.J.G. Fait, H.-J. Lunk, M. Feist, M. Schneider, J.N. Dann, and T.A. Frisk, Thermochim.Acta, **469**, 12-22 (2008)

26. Y. Muraoka, J.-C, Grenier, S. Petit, and M. Pouchard, *Solid State Sciences*, **1**, 133-148 (1999)

27. K. Nakamoto, *Infrared and Raman Spectra of Inorganic and Coordination Compounds,* John-Wiley and Sons, Inc., 3rd edition, (1978)

28. P.C.H. Mitchell, S.F. Parker, A.J. Ramirez-Cuesta, and J. Tomkinson, *Serie on Neutron Techniques and applications – Vol.3: Vibrational Spectroscopy with Neutrons,* pp. 185-195,World Scientific Publ.Co.Pte.Ltd., (2005)

29. N.W. Ockwig, R.T. Cygan, M.A. Hartl, L.L. Daemen, and T.M. Nenoff, *J.Phys.Chem.*, **C 112**, 13629-13634 (2008)